Soft Matter

PAPER

View Article Online
View Journal | View Issue

Cite this: *Soft Matter*, 2021, **17**, 3672

Biofilm mechanics in an extremely acidic environment: microbiological significance†

Virginia Souza-Egipsy, *[a] Juan F. Vega,[a] Elena González-Toril[b] and Ángeles Aguilera[b]

A variety of natural biofilms were collected from an extremely acidic environment at Río Tinto (Spain). In order to provide insights into the structure–function relationship, the microstructure of the biofilms was explored using low temperature scanning electron microscopy (LTSEM) in combination with rheological analysis. The creep-recovery experiment results have demonstrated the typical behaviour of viscoelastic materials that combine both elastic and viscous characters. The LTSEM visualization and rheological characterization of biofilms revealed that the network density increased in bacterial biofilms and was the lowest in protist *Euglena* biofilms. This means that, in the latter biofilms, a lower density of interactions exist, suggesting that the whole system experiences enhanced mobility under external mechanical stress. The samples with the highest dynamic moduli (*Leptospirillum–Acidiphilium, Zygnemopsis, Chlorella and Cyanidium*) have shown the typical strain thinning behaviour, whereas the *Pinnularia* and *Euglena* biofilms exhibited a viscous thickening reaction. The *Zygnemopsis* filamentous floating structure has the highest cohesive energy and has shown distinctive enhanced resilience and connectivity. This suggests that biofilms should be viewed as soft viscoelastic systems the properties of which are determined by the main organisms and their extracellular polymeric substances. The fractional Maxwell model has been found to explain the rheological behaviour of the observed complex quite well, particularly the power-law behaviour and the characteristic broad relaxation response of these systems.

Received 6th November 2020,
Accepted 12th February 2021

DOI: 10.1039/d0sm01975e

rsc.li/soft-matter-journal

1. Introduction

Highly acidic extreme environments are relatively scarce worldwide and are generally associated with volcanic activity and mining operations. The oxidation and dissolution of the sulfidic minerals exposed to oxygen and water results in acid production, and the process is greatly enhanced by microbial metabolism.[1–3] At the same time, low pH facilitates metal solubility in water, particularly cationic metals, and thus extremely acidic water tends to have high concentrations of heavy metals. However, in spite of the apparent hostility of these habitats, they contain a higher level of biodiversity and biomass than expected.[4] Most of the microbial communities found in extreme environments are distributed and assembled in extensive biofilms. Natural biofilms are organized multicellular systems with a structural and functional architecture that influences metabolic processes, response to nutrients, predation and other factors of the ecosystem.[5]

Biofilms are a typical feature in the acidic streams of the Río Tinto upper zone, where sediments can be covered by a yellow, brown or greenish mucous layer wherever the water flow is not too strong.[6,7] In addition, floating bacterial biofilms on the surface of the water[8] and forming part of photosynthetic eukaryotic biofilms[9] have been also described. Their microbial diversity and extracellular matrix composition have been previously studied.[10–12] A variety of microorganisms located in these colourful biofilms have been identified, from unicellular algae, such as *Pinnularia*, *Chlorella* and *Cyanidium*, to filamentous green algae, such as *Klebsormidium* and *Zygnemopsis*. Protists such as *Euglena*, fungi and bacteria are also an important part of these biofilms. In the natural environment, biofilms are able to form patches in streams without a clear distribution pattern. They form a matrix at the sediment–surface interface or develop streamers floating on the water but anchored to a surface. It has not been possible to grow these biofilms under controlled culture conditions, which makes their collection from their natural environment the only way to study them.

While several studies on the composition of extracellular polymeric substances (EPS) from extremophilic bacteria have been performed to date,[13,14] little is known about the relationship of the matrix with the rheological features of the different

[a] *BIOPHYM, Department of Macromolecular Physics, Instituto de Estructura de la Materia (IEM-CSIC), c/Serrano 113 bis, 28006, Madrid, Spain. E-mail: virginia.souza-egipsy@csic.es*
[b] *Centro de Astrobiología (CSIC-INTA), Carretera de Ajalvir Km 4, Torrejón de Ardoz, 28850, Madrid, Spain*

† Electronic supplementary information (ESI) available. See DOI: 10.1039/d0sm01975e

eukaryotic biofilms in their natural environment. Biofilms are in general heterogeneous systems composed of microorganisms and macromolecules embedded in water that do not behave as purely viscous fluids or purely elastic solids. The cohesive forces keeping these microorganisms in contact provide structural stability to the biofilm and give rise to their characteristic viscoelasticity. This specific mechanical feature essentially arises from the structural organization of the biofilms. A deep characterization of the microstructure of these complex systems requires studying not only their rich morphological features, but also their rheological properties, that is, the response of the biofilms to external forces or deformations. A comprehensive synthesis of the knowledge surrounding this specific topic can be found in recent reviews,[15–18] which focused mainly on the most frequent bacterial biofilms. In this context, agreement among researchers exists on how little is known about the impact of mechanical history in the coupling among microorganisms forming the biofilms and thus how this coupling affects their morphology, physiology, distribution and interactions with the environment. Since most of these previous studies have focused exclusively on the rheological properties of prokaryotes, references related to the rheological features of natural eukaryotic biofilms are even scarcer.

Biofilms at Río Tinto are pervasive in particular extreme conditions and knowledge of their mechanical properties would be useful in order to understand their ecological characteristics. From a biological perspective, these biofilms are complex structures, comprising microbial cells embedded in a matrix of EPS as polysaccharides, proteins, humic acids and minerals.[10–12] From a physical perspective, biofilms are viscoelastic materials, behaving similarly to polymer gels. More specifically, a number of studies suggest that prokaryotic biofilms behave as viscoelastic liquids.[19–22] However, very little is known about the specifics of the possible mechanical traits that characterize different types of eukaryotic biofilms. For instance, yeast biofilms were determined to be viscoelastic materials with a predominant solid-like behaviour.[23,24] Despite the existence of several marine species of polysaccharide-producing microalgae with commercial interest, little is known about the relationship between their conformation and structure, and their physicochemical properties, including rheological behaviour.[25] Whether the goal is to encourage or discourage biofilm accumulation, detachment is one of the key determinants of how much biofilm accumulates. Biofilm detachment and its correlation to the mechanical properties of the biofilm are indisputably important.[19]

The roles of the EPS in the functioning of biofilms have been discussed in detail,[26,27] although their fine structure and composition is less well understood. Microscopic techniques, such as confocal laser scanning microscopy (CLSM), have provided a description of the biofilm structure and its microbiological diversity[28] as well as its biochemical composition.[29] The role of water in the highly hydrated matrix present in biofilms has been difficult to describe using conventional electron microscopic techniques because of the desiccation required by high-vacuum conditions. In 1986, Paterson *et al.* pioneered the use of low temperature scanning electron microscopy (LTSEM) in the formation of sediment biofilms.[30] LTSEM allows the observation of liquid rich materials in a frozen state. In the LTSEM technique, water is vitrified with liquid nitrogen under vacuum and maintained at very low temperature. It is an indispensable tool for preserving the *in situ* organic texture under highly hydrated conditions and has been successfully used to characterize microbial sediments[31,32] and microbial mats[33] as well as phytoplankton marine aggregates.[34]

The main purpose of this study is to provide comparative data on biofilms from extremely acidic natural streams. The results from this study contribute to the understanding on how different natural biofilms react to mechanical stimuli in an extremely acidic environment. Differences among species would lead to a better interpretation of what factors control their ecological niche distribution.

2. Materials and methods

2.1. Study site, sample collection and biofilm microbial composition

Six microbial biofilms from two sampling points (CEM 37°42′8″ N/6°33′31″ W and ANG 37°43′15″ N/6°33′10″ W) along the upper stream of Río Tinto (SW, Spain) were selected for *in situ* water measurements and epilithon collection (Fig. 1 and Table 1).

A general description of the river hydrochemical parameters and the microbial diversity and natural thickness of biofilms has been reported previously.[6,7] Biofilm samples were taken from the field including their soil substrate in June 2019 and

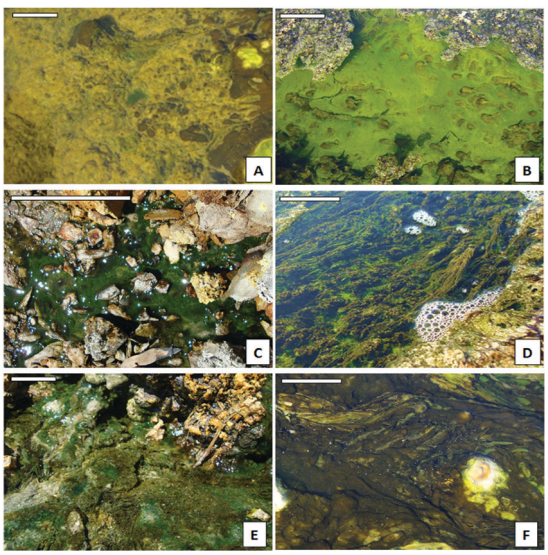

Fig. 1 (A) General aspect of *Leptospirillum–Acidiphilium* bacterial biofilms (CEM-Bac). (B) Detailed image of brilliant green *Euglena mutabilis* biofilms (CEM-Eug). (C) Aspect of the patched green biofilms of *Chlorella* sp. (ANG-Chlo). (D) General view of the floating filaments of *Zygnemopsis* sp. (CEM-Zyg). (E) General aspect of green-blue *Cyanidium* sp. biofilms (CEM-Cya). (F) General aspect of brown *Pinnularia* sp. biofilm samples (CEM-Dia). Scale bar = 10 cm.

Table 1 Description of the biofilm samples

Sampling site	Sample name	Species composition	pH	Redox (mV)	Cond (mS cm^{-1})	T (°C)	O_2 (ppm)
ANG	ANG-Chlo	*Chlorella* spp.	1.7 ± 0.2	471 ± 16	30 ± 3	24 ± 1	1.7 ± 0.7
CEM	CEM-Bac	*Leptospirillum* spp. *Acidiphilium* spp.	2.3 ± 0.1	446 ± 15	11 ± 3	17 ± 2	2.8 ± 0.2
	CEM-Cya	*Cyanidium* spp.	2.2 ± 0.2	450 ± 14	13 ± 2	18 ± 1	2.9 ± 0.1
	CEM-Dia	*Pinnularia* spp.	2.3 ± 0.2	443 ± 11	14 ± 1	17 ± 3	2.5 ± 0.4
	CEM-Eug	*Euglena mutabilis*	2.1 ± 0.2	448 ± 11	12 ± 3	18 ± 1	2.8 ± 0.2
	CEM-Zyg	*Zygnemopsis* spp.	2.2 ± 0.2	456 ± 10	12 ± 1	19 ± 2	2.7 ± 0.5

Mean and standard error of water physical parameters at each sampling site.

placed in 6-well culture plates (Corning, USA) for transport and conservation. This method of collection was previously used and helped to maintain the structure of the biofilms from the field to the laboratory.[7] At this time of the year the biofilms acquired their highest development stages since spring.[6]

The samples were kept in the dark at 5 °C for six days during the analyses. The biofilm species composition was examined by direct microscopic observation using a Zeiss Axioscope 2 equipped with phase-contrast. Bacterial biofilm identification was carried out by fluorescence *in situ* hybridization (FISH). Hybridization and staining with DAPI (4′,6-diamidino-2-phenylindole) were carried out as previously described.[35] Cy-3 labelled probes were provided by Molecular Probes (Thermo Fisher Scientific). Detailed information on the sequences and oligonucleotide probes is available from previous studies.[1,2,8,9] The Citifluor mounting medium (Citifluor Ltd, UK) was added to the preparations to avoid fluorescence fading. An Axioskop microscope (Zeiss, Germany) equipped with the proper filter set was used to visualize the FISH results. *In situ* measurements of water conductivity, temperature (conductivity meter: Orion 122, Orion Research, USA), redox and pH (pH meter: Crison 506 pH/Eh), and oxygen (Orion 810 oxymeter) were made in triplicate.

We selected and named the biofilms according to the microbial composition of their main species, and the color features were also useful to distinguish them in the field. Three biofilms were mainly composed by microalgae: green *Chlorella* spp. (*Chlorophytes*), blue-green *Cyanidium* spp. (*Rhodophytes*), and brown *Pinnularia* spp. (*Bacillariophytes*). We selected also a biofilm of a photosynthetic protist, dark green *Euglena mutabilis* (*Euglenozoa*), and the floating green filamentous algae *Zygnemopsis* spp. (*Streptophyta*). Additionally, a brownish bacterial biofilm composed mainly by *Leptospirillum* spp. (*Nitrospirae*) and *Acidiphilium* spp. (*Proteobacteria*) was also analyzed. Detailed information about the composition of the studied samples is available from previous works.[6–12]

2.2. Low temperature scanning electron microscopy

In some cases, pieces of the biofilm attached to the mineral substrate were used but in others due to the higher thickness only superficial material was used. A precise description of the structure and thickness of the different biofilms has been the focus of a previous study.[7] The material from each natural biofilm was selected using a spatula and mounted in a cryo-holder at room temperature. The samples were immediately plunge-frozen in slush nitrogen and directly transferred into the cryo-chamber pre-cooled to −180 °C *via* an airlock transfer device. The frozen material was then fractured inside the cryo-chamber with a cooled blade to observe a fresh fractured cross section of the biofilm. After fracturing, the sample was placed in the SEM-chamber where it was slowly heated to −90 °C for 2 min to sublimate the first superficial microns of water. This step aids the observation of the ultrastructural elements and permits the identification of the water fraction and the confirmation of its location. The specimen was then returned to the cryo-chamber and sputter-coated with gold for 2 min 15 s at 10 mA. The observation and the recording of images were done at −150 °C at an acceleration voltage of 10–15 kV. The instrument used was a CT1500 Cryotrans system (Oxford Instruments) mounted on a Zeiss 960 SEM (Centro de Ciencias Medioambientales, CSIC, Madrid).

2.3. Rheological measurements

Small amplitude strain sweeps, frequency sweeps and creep-recovery during constant stress experiments were carried out in order to locate the linear viscoelastic region and to determine the basic linear viscoelastic properties of the biofilms. The experiments were performed with a Bohlin CVO stress-controlled rheometer at room temperature (T = 22 °C) using parallel plates (25 mm diameter). The superficial part of each sample was carefully deposited over the lower plate of the rheometer with the help of a spatula. The biofilms had different natural thicknesses but we used only the superficial material, avoiding the material in contact with the soil substrate to fill a gap setting of 500 μm between the plates. The upper plate was lowered until the normal force was approximately 1 N. The samples were allowed to equilibrate for at least 5 min. Measurements were performed for 3 to 5 independent samples. The values were averaged and the relative standard deviation (RSD) was obtained for each case. The results shown correspond to those averaged values.

Three different experiments were performed:

1. Location of the linear viscoelastic region by measuring the dynamic moduli, G' and G'', as a function of strain amplitude at a frequency of 1 Hz.

2. Frequency sweep experiments in the strain-controlled mode at low strains selected in 1, to ensure that the biofilm response remained in the linear region and then the structure was not destroyed during the experiment. The dynamic properties such as storage and loss moduli, G' and G'', were determined by sweeping across the frequency range from 0.02 to 20 Hz.

3. Creep-recovery experiments at different shear stresses, σ. There were performed in the linear viscoelastic region in order to obtain the time evolution of the creep and recovery compliance, J_c and J_r, respectively. The applied stress depended on the nature of the samples. The previous experiments in (1) aided to select the values of the suitable shear stress applied in each case. Recovery experiments were performed after creep times, t_c = 125, 250 and 500 s.

3. Results

3.1. Low temperature scanning electron microscopy

The observations under LTSEM revealed the ultrastructure of the different samples studied, except for the filamentous algae *Zygnemopsis* (CEM-Zyg). The size of the filaments made it very difficult to maintain the natural structure for observation under the microscope. At low magnification the bacterial biofilms (CEM-Bac) showed a compact structure with clumps of cells (Fig. 2A). The bacterial biofilms became more compact and exhibited a more intertwined fibrous network of EPS (arrows in Fig. 2B). The biofilms of *Chlorella* (ANG-Chlo) showed a web structure consisting of thin threads organized around the cells (Fig. 2C), with the strand-like structures forming an intertwined fibrous network. A detailed view of the biofilm over the surface of the sediment revealed a web of homogeneously distributed fibrillar material. This fibrillar material appeared to be covered with minerals (arrows Fig. 2D). In these biofilms the fibrillar material made delineated pores. *Euglena* biofilms (CEM-Eug) showed poor network development with less fibrillar EPS (Fig. 2E), although the fibrillar material was present surrounding each individual cell (arrow in Fig. 2F).

The ultrastructure of *Pinnularia* (CEM-Dia) (Fig. 3A and B) and *Cyanidium* (CEM-Cya) (Fig. 3C and D) biofilms showed a similar distribution of the fibrillar material, exhibiting a more open structure with a less intertwined network compared to *Chlorella* biofilms. In the *Pinnularia* biofilm, it was possible to observe the links between capsular EPS outside the frustule and the fibrillar network (arrow in Fig. 3B). Mineral deposits were frequent on *Cyanidium* cell walls (arrow in Fig. 3D).

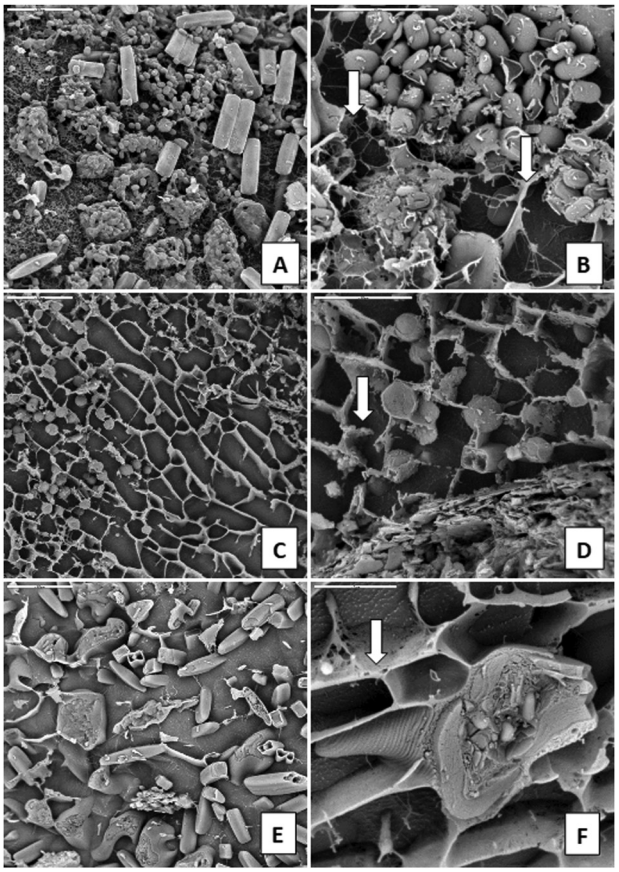

Fig. 2 (A) Bacterial biofilms are densely packed forming clumps (CEM-Bac). Some diatom frustules are present. Scale bar = 20 μm. (B) Detailed image of clumps of bacteria. The arrow points to the EPS aspect in areas where the water has been sublimated. Scale bar = 10 μm. (C) Detailed aspect of a cross-sectioned *Chlorella* biofilm (ANG-Chlo). Scale bar = 20 μm. (D) Detailed image of the web formed by the EPS around cells in contact with the substrate below. Scale bar = 10 μm. (E) *Euglena* biofilm cross section (CEM-Eug). Scale bar = 20 μm. (F) Detailed image of the EPS surrounding one individual (arrow). Scale bar = 5 μm.

3.2. Rheology: strain amplitude sweeps

The curves of storage, G', and viscous, G'', moduli *versus* amplitude strain, γ, are shown for the selected samples in Fig. 4. These curves are extracted from the dynamic amplitude strain sweeps (see Fig. S1 of the ESI†). At low values of strain, G' remains constant at a characteristic G_c' value, which is different for each sample. The range within G' remains constant with γ being defined as the linear viscoelastic range. The linear viscoelastic region extends up to a critical value γ_c. In this

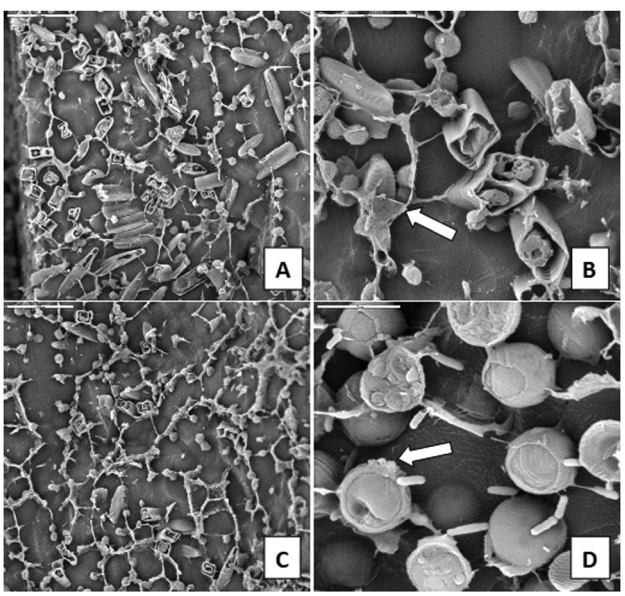

Fig. 3 (A) Diatom biofilm cross section (CEM-Dia). Bar = 50 μm. (B) Detailed image of the EPS connecting diatom frustules in the biofilm (arrow). Bar = 10 μm. (C) *Cyanidium* biofilm cross section (CEM-Cya). Bar = 20 μm. (D) Detailed image of the *Cyanidium* biofilm and the associated bacteria. The arrow points to mineral deposits. Scale bar = 5 μm.

range, the rheological properties reflect the specific microstructure of the samples. A further increase of γ results in a decrease in G', which indicates the disruption of the interactions among the components of the samples above γ_c.

The values of G_c' and γ_c were estimated using the tangent method depicted using solid lines in Fig. 4. The values listed in Table 2 are the averages from 3 to 5 measurements (Fig. S1, ESI†). A disparity of orders of magnitude in the specific values of G_c' and γ_c is observed.

It should be noted that a subsequent strain sweep on the same sample yields the same result (open symbols in Fig. 4), which means that the structure is fully recovered after the first test. The experiments are highly repeatable, indicating a fast recovery of the structural changes. This seems to be a general behaviour shown by all the samples. The samples with the highest values of dynamic moduli (CEM-Bac, CEM-Zyg, ANG-Chlo, CEM-Cya) have shown the typical strain thinning behaviour (G' and G'' decreasing with γ above the critical value, γ_c). The behaviour observed in the case of diatom and protist biofilms (CEM-Dia and CEM-Eug) is different. In these cases, especially in the diatom biofilm, a weak strain overshoot in G'' (viscous thickening) is clearly observed.

4. Rheology: oscillatory shear and creep-recovery

Shear dynamic moduli and creep-recovery of *Pinnularia* and *Euglena* biofilms could not be measured using our experimental setup, which is likely because of their softness and a dehydration process that takes place in these samples in a few minutes. The dynamic moduli G' and G'' of the rest of the samples (CEM-Bac, CEM-Zyg, ANG-Chlo and CEM-Cya) have been obtained as a function of the frequency, ω, in the linear viscoelastic region (below the corresponding critical value γ_c in Table 2). The results obtained for these samples are shown in Fig. 5. The elastic component of the complex modulus G' is regularly higher than the viscous component G'', over the experimental frequency range, which indicates that the samples behave like weak gels. This implies the presence of a network structure established among the microorganisms and the EPS consistent with LTSEM images. In the frequency range explored G' exhibits the typical power-law with frequency ($G' \sim \omega^n$), but G'' passes through a local minimum, less pronounced as the softness of the sample increases from CEM-Bac to CEM-Cya. The data presented in Fig. 6 correspond to the creep (Fig. 6A, creep time t_c = 300 s) and creep-recovery experiments (Fig. 6B, creep time t_c = 125 s) obtained for the samples.

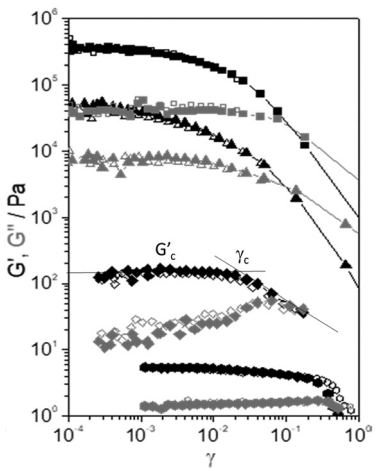

Fig. 4 Elastic modulus (G', black symbols) and viscous modulus (G'', grey symbols) *versus* strain amplitude, γ, of the selected samples: (■) CEM-Bac, (▲) ANG-Chlo, (♦) CEM-Dia, and (⬣) CEM-Eug.

Table 2 Basic rheological properties at T = 22 °C. Characteristic elastic modulus, G_c', critical shear strain, γ_c, and cohesive energy, E_c

Sample	G_c' (kPa)	γ_c	E_c (J m^{-3})	RSD
ANG-Chlo	47.3	0.006	0.86	0.37
CEM-Bac	430	0.003	1.95	0.09
CEM-Cya	11.4	0.007	0.26	0.40
CEM-Dia	0.11	0.020	0.021	0.08
CEM-Eug	0.008	0.05	0.012	0.12
CEM-Zyg	80.0	0.01	4.00	0.20

For each sample, the average value of three to five replicates and its relative standard deviation (RSD) are shown.

The results have confirmed that the response under constant shear stress is also power-law time dependent, $J_c(t) \sim t^n$. The creep and recovery results have demonstrated the typical behaviour of viscoelastic materials that combine both elastic and viscous characters. The linearity of the strain response in all measurements has been assessed by performing experiments at three different stress levels below the critical shear stress listed in Table 2 (Fig. 6A). All samples show a similar response in the recovery step, as observed in Fig. 6B. The curves exhibit (i) an instantaneous elastic compliance at t = 0, (ii) a time dependent viscous compliance up to t_c, (iii) an instantaneous recovery when the stress is removed just after t_c, and finally (iv) an unrecoverable compliance at the end of the experiment at t_r.

Expressing the relationship between external stresses and deformation in constitutive laws is an important step in predicting and ultimately describing the phenomena related to the microstructure of the biofilms and their ecological mechanics. The Burgers model has been widely used to understand rheological experiments in biofilms, mainly in creep and creep-recovery experiments.[21,36] This model combines elastic and viscous mechanical elements which can be represented as springs and dashpots, respectively (Fig. S2 in the ESI†). The specific combination of the Burgers model leads to a constitutive equation of constant coefficients that establishes the relation between stress and strain as a function of time (equation (S1), ESI†). This equation should apply for different experiments (dynamic, creep and recovery) using the same set of coefficients. We have applied the model using the corresponding equations (see the ESI†) and observed that it is not able to describe the whole set of experiments in these power-law materials. The results obtained in the case of the CEM-Zyg sample in dynamic and creep-recovery experiments are shown in Fig. 7. The Burgers model, represented by the dotted lines, particularly fails in the

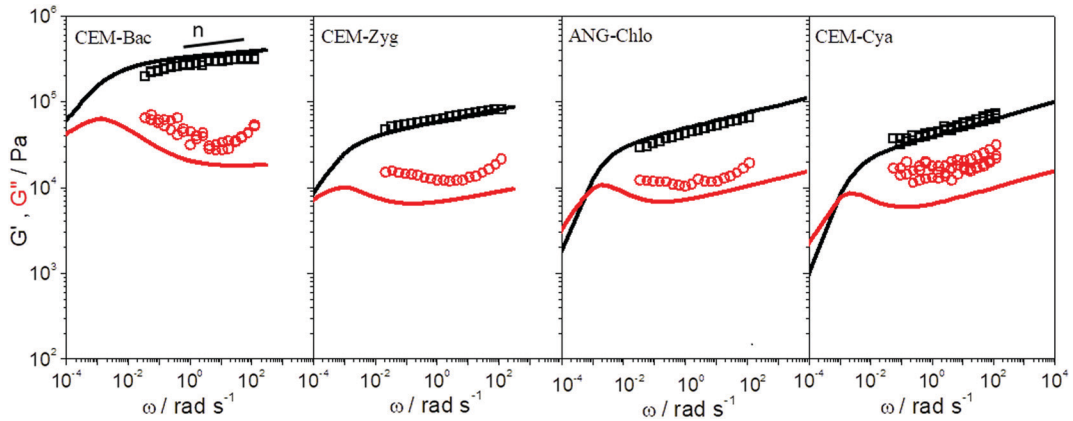

Fig. 5 Elastic (G', squares) and viscous (G'', circles) moduli *versus* angular frequency, ω, of the samples studied. Fractional Maxwell model (solid lines).

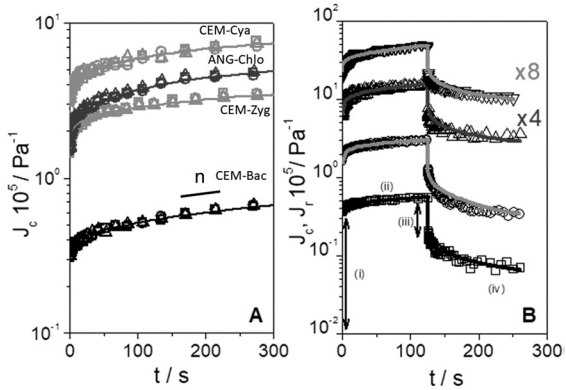

Fig. 6 (A) Creep compliance, J_c, *versus* time of the samples studied at different shear stress values, σ: (□ 1000 Pa, ○ 500 Pa, △ 250 Pa) CEM-Bac; (□ 600 Pa, ○ 300 Pa, △ 150 Pa) CEM-Zyg; (□ 200 Pa, ○ 150 Pa, △ 75 Pa) ANG-Chlo; (□ 60 Pa, ○ 30 Pa, △ 15 Pa) CEM-Cya. Fractional Maxwell model (solid lines). (B) Creep, J_c, and recovery, J_r, compliance at the highest stress and t_c = 125 seconds, of the samples studied: (□) CEM-Bac, (○) CEM-Zyg, (△) ANG-Chlo, and (▽) CEM-Cya. Fractional Maxwell model (solid lines).

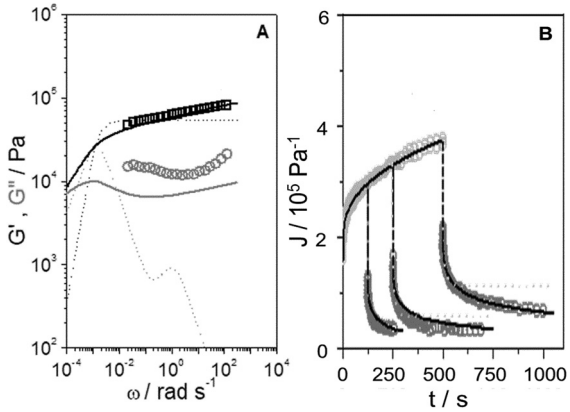

Fig. 7 (A) Elastic modulus (G', □ black symbols) and viscous modulus (G'', ○ grey symbols) *versus* angular frequency, ω, of the CEM-Zyg sample. Burgers model (dotted lines). Fractional Maxwell model (solid lines). (B) Creep compliance (J_c, light grey symbols) and recovery compliance (J_r, dark grey symbols) *versus* time of the CEM-Zyg sample at different creep times, t_c = 125, 250 and 500 s. Burgers model (dotted lines). Fractional Maxwell model (solid lines).

case of the dynamic measurements (Fig. 7A) and the recovery tests (Fig. 7B) performed for long creep times. This failure is likely due to the simplicity of the Burgers model, providing a clear indication of the broad relaxation spectrum of relaxation processes related to the specific microstructure composing these power law materials.[37]

In order to describe this broad response, it is necessary to add elements to provide additional relaxation modes. However, this procedure generates more parameters without a clear physical meaning. To avoid this problem, a constitutive framework based on fractional derivatives within the Scott–Baird approach is used.[37–40] Please refer to the works of McKinley *et al.*[37,39,40] and to the ESI† for details. We have extracted the parameters (see Table 3) from the creep data by fitting the experimental results in Fig. 6A to the corresponding equation for CEM-Bac, CEM-Zyg, ANG-Chlo and CEM-Cya samples and used them to estimate the response of the material in the other experiments, *i.e.* recovery and dynamic tests. The reader is referred to the ESI† where the equations are shown in detail. The agreement between experiments and predictions over the different testing protocols indicates that the fractional description represents a constitutive model whose coefficients, given by the characteristic modulus and relaxation time, G_0 and λ_c, are the actual material properties with a physical meaning.

The coefficients extracted from the application of the model to the creep experiments explain quite well both the recovery and dynamic tests, as can be seen in Fig. 5–7 (solid lines).

Table 3 Parameters of the fractional Maxwell model

Sample	$\mathbb{V}$ (kPa s$^{\alpha}$)	α	$\mathbb{G}$ (kPa s$^{\beta}$)	β	G_0 (kPa)	λ_c (s)
ANG-Chlo	7220	0.80	50.0	0.08	27.0	1050
CEM-Bac	11 800	0.54	271.4	0.03	217.6	1630
CEM-Cya	5100	0.83	34.1	0.10	20.2	900
CEM-Zyg	8400	0.67	58.9	0.07	32.8	3930

5. Discussion

Concerning the stability and resilience of the systems under study, the analysis of rheological behaviour and microscopy in the Rio Tinto samples studied has revealed that the increases in stiffness and cohesive energy are complemented by higher network formation. It is interesting to note that as the stiffness, G_c', of the sample increases, the critical strain, γ_c, steeply decreases (see Table 2). These rheological properties can be quantitatively analysed in terms of inter-particle forces.[41] In these complex systems a microstructure exists, together with a cohesive energy, E_c, that retains the microorganisms together, conforming a characteristic distribution or microstructure, which should dictate the rheological behaviour. The cohesive energy, E_c, which is the energy required to keep the microorganisms aggregated, should command the ecological mechanics for survival. The values can be obtained through the parameters that describe the transition between the linear and non-linear regions, the critical strain, γ_c, and the elastic modulus value of the linear viscoelastic region, G_c', as[42,43]

$$E_c = \int_0^{\gamma_c} \sigma \mathrm{d}\gamma \quad (1)$$

where γ_c is the critical strain which results in the disruption of the network and σ is the stress in phase with the strain, γ, then $\sigma = G'\gamma$. As G' remains constant in the linear viscoelastic region, $G' = G_c'$, substitution in eqn (1) leads to this simple relationship:

$$E_c = \frac{1}{2} G_c' \gamma_c^2 \quad (2)$$

The large difference in E_c values (two orders of magnitude in Table 2) indicates strong microstructural and/or compositional differences in the biofilms studied. The results suggest that the *Zygnemopsis* sample and biofilms of *Leptospirillum–Acidiphilium*, *Chlorella* and *Cyanidium* are structurally stronger than *Pinnularia* and *Euglena* biofilms.

The case of *Zygnemopsis* is remarkable, as its morphology and ecology are clearly different from those of the biofilms and it has the highest value of cohesive energy and an extremely long relaxation time (close to 4000 s). *Zygnemopsis* forms bundles of filaments floating on the surface of the water only attached slightly to the substrate.[6] It has been reported that these bundles of filamentous algae showed higher amounts of total EPS when collected from Río Tinto than from other extreme environments.[12] The presence of a significantly larger amount of colloidal EPS was related to the presence of heavy metals in the waters. In addition, these floating communities showed a light saturation model related to their more exposed location in the environment.[44] Their higher photosynthetic productivity during the summer months could explain their capacity to have a higher amount of EPS. Of course, a higher concentration of EPS, which creates a more complex interconnected structure together with the specific morphology and assembly of the microorganisms, should contribute to the extremely long relaxation time measured. Please note that the higher density of interactions given by E_c does not mean a direct increase of the stiffness with respect to the biofilms, but rather a higher critical strain to failure under high levels of stress (see Table 2).

The results obtained in the bacteria-dominated biofilm indicate that it presents the highest stiffness and mechanical stability. This biofilm is characterized by significantly high modulus, cohesive energy, and relaxation time (around 1600 s) corresponding to the closely packed and intertwining network observed in LTSEM. It should be noted that in this case the value of the modulus, one order of magnitude higher than those in the rest of the samples, is a direct consequence of the closely packed morphology and the density of interactions. Bacterial biofilms have been described as structured multispecies communities that differ profoundly from those of planktonically grown cells of the same species.[45]

In the case of *Chlorella* biofilms, the microstructural study showed a matrix formed by an intertwined material (Fig. 2C and D) with the highest E_c values among the unicellular algae. *Cyanidium* biofilms exhibited a more open structure with a less intertwined network than *Chlorella* biofilms, correlated with less than half of the cohesive energy (Fig. 3C and D). These systems also show lower values of λ_c than *Zygnemopsis* and *Leptospirillum–Acidiphilium* biofilms, *i.e.* around 1000 s. These values are however still high, being a signature of certain structural stability under external forces. In fact, *Chlorella* and *Cyanidium* biofilms from Río Tinto have shown higher amounts of EPS than other extreme environments related to higher concentrations of heavy metals in these stream waters.[12]

Pinnularia (Fig. 3A and B) and *Euglena* (Fig. 2E and F) biofilms have shown the lowest values of both moduli and cohesive energy (see Table 2). The low E_c values mean a lower density of interactions among the components, inferring the whole systems with enhanced mobility under external mechanical stress. Then, these biofilms represent the softer and mobile end of the biofilms studied here, which is again consistent with LTSEM results, as the biofilms showed a more open structure with a less intertwined network of EPS than *Cyanidium* and *Chlorella* biofilms. Diatoms and euglenoids are among the organisms that exhibit horizontal and vertical patterns of migration in their ecological niches.[46] These changes in the distribution and orientation of the diatoms in the biofilm have an influence on the acclimation of cells under excess light[47] and may be affected by their rheological properties. In the case of euglenoids their cell wall is flexible and the secretion of EPS will help in their movement.

Then, as a general observation it should be noted that as the network density increases, as observed in LTSEM images (Fig. 2 and 3), the value of E_c also does. Moreover, a relationship may be anticipated between the cohesiveness of the samples given by E_c and the characteristic relaxation time, λ_c, obtained from the fit to the fractional Maxwell model (see Tables 2 and 3). Shaw *et al.*[22] reported that the overall characteristic time, λ_c, in a biofilm collection remains constant at about 1110 s, the minimum and maximum values being 350 and 2600 s, respectively. The authors argued a connection between this characteristic rheological value and the bacterial doubling times in growing

biofilms. This connection may have survival significance for the microorganisms, as this characteristic time is the period over which a biofilm can both grow and respond to external stresses. The results for λ_c obtained in the samples studied here are within the range observed by Shaw *et al.*, except for the filamentous algae *Zygnemopsis* sample, which exhibits a characteristic time 3–4 times higher than the average. From our results, it is clear that as λ_c increases the required energy to disturb the network also does. This relationship between E_c and λ_c suggests a more complex connection between the microstructure/rheology and the survival time, which is likely related to specific features of the EPS and to the interactions with the microorganisms that deserve a more specific study. It is important to recall that the rheological properties are determined by parameters like the size and shape of the microorganisms and the interacting forces between them. However, these properties are also modulated by the surrounding EPS and of course by the composition, molecular structure (topology) and volume fraction of each of the components.

It should be noted that the samples with the highest values of the dynamic modulus, cohesive energy and relaxation time (*Leptospirillum–Acidiphilium*, *Zygnemopsis*, *Chlorella* and *Cyanidium*) have shown the typical strain thinning behaviour most widely observed in polymeric solutions and melts.[48] The origin of this behaviour is associated with the orientation of the microstructure with the flow direction, which reduces the local drag as a consequence of a decreased density of interactions. On the contrary, in the biofilms with motile organisms (*Pinnularia* and *Euglena*), the strain-induced microstructure is able to resist the deformation, and G'' increases up to a maximum value, giving rise to a shear thickening behaviour. After the maximum is reached, G'' starts to decrease as γ increases further due to the disruption of the structure.[49] It is noteworthy that these softer biofilms have shown a distinctive shear thickening behaviour, reported in the literature in a large variety of systems such as carbohydrate hydrocolloids[50] and colloidal microgels.[51] This specific mechanical feature allows them to withstand eventual external stresses while maintaining their dimensional stability. In this respect it should be noted that a key outstanding question in the study of the physics of complex transient networks like those studied in this work is the fundamental molecular origin of the observed viscous thickening phenomenon.[52] A detailed study of the nature of the EPS is highly desirable in this specific case, as the molecular weight and, more remarkably, the molecular topology (branching) may play a fundamental role in the observed behaviour.

As a final remark, it is worth highlighting the observation that, among the biofilms, the prokaryotic bacteria have shown the highest values of shear modulus and relaxation time. The value of the modulus in this specific case is orders of magnitude higher than that observed in eukaryotic systems (see Tables 2 and 3). The characteristic crowd of highly interconnected microorganisms is the main cause of this behaviour, and this clearly contrasts with the behaviour observed in eukaryotic systems that a more open microstructure gives rise to systems with greater deformability and therefore mobility.

6. Conclusions

Biofilms from Río Tinto have shown an extraordinary microstructural and rheological variability. The difference among the biofilms manifests itself in stiffness values that may vary by five orders of magnitude. This variability can be described through the cohesive energy, which defines the density of interactions of the transient network that characterizes each of the biofilms. The strongest and densest networks (*Leptospirillum*/*Acidiphilium*, *Chlorella*, and *Cyanidium*), having a low ability to deform, have shown a high cohesive energy, which clearly contrasts with those soft biofilms with a lower density of interactions (*Pinnularia* and *Euglena*). *Zygnemopsis* has shown distinctive enhanced resilience and connectivity. Both characteristics should be connected to the filamentous morphology of these microorganisms and also to the previously reported higher concentration of extracellular polymeric substances, which is a unique signature of the Río Tinto ecosystem. Interestingly, the most mobile *Pinnularia* and *Euglena* biofilms display a specific mechanical feature, such as viscous thickening, which should allow these systems to withstand eventual external stresses while maintaining their dimensional stability. The fractional Maxwell model has been found to be quite a versatile approach to explain the broad relaxation spectrum of the samples. In fact, it has allowed us to obtain basic viscoelastic parameters of the networks, such as elastic modulus and characteristic time. The characteristic times are located around 15–26 min as previously reported in a large collection of biofilms, except for *Zygnemopsis*. This system has shown a quite large characteristic time of 1 h, which is likely due to the specific morphology of the microorganisms, microstructure and EPS composition. It must be noted that a correlation is found between the cohesiveness and relaxation time of the networks, pointing towards a complex connection between microstructure, rheology and survival time. The eukaryotic biofilms composed of highly mobile microorganisms have shown the lowest values of shear modulus, relaxation time and cohesiveness.

Authors' contributions

VS-E: conceptualization, investigation, writing – original draft. JFV: methodology, investigation, formal analysis, writing – original draft. AA: conceptualization, resources, writing – review & editing, supervision, funding acquisition. EG-T: resources, editing, funding acquisition.

Conflicts of interest

The authors declare that they have no known competing financial interests or personal relationships that could have appeared to influence the work reported in this paper.

Acknowledgements

VS-E wishes to acknowledge F. Pinto at the CCMA-CSIC for his lifetime dedication to electron microscopy. The TEM-BIOPHYM Service at the IEM-CSIC is acknowledged for granting the use of the facilities. This work was funded by the Spanish Science and

Innovation Ministry (grants CGL2017-92086-EXP, RTI2018-094867-BI00 and PID2019-104205GB-C22).

References

1 E. González-Toril, E. Llobet-Brossa, E. O. Casamayor, R. Amann and R. Amils, *Appl. Environ. Microbiol.*, 2003, **69**, 4853–4865.
2 E. González-Toril, F. Gómez, N. Rodríguez, D. Fernández-Remolar, J. Zuluaga, I. Marín and R. Amils, *Hydrometallurgy*, 2003, **71**, 301–309.
3 A. García-Moyano, E. González-Toril, A. Aguilera and R. Amils, *FEMS Microbiol. Ecol.*, 2012, **81**, 303–314.
4 B. D. Johnson and A. Aguilera, in *Encyclopedia of Microbiology*, ed. M. Schaechter, Elsevier, Oxford, 2019, pp. 206–227.
5 L. Hall-Stoodley, J. W. Costerton and P. Stoodley, *Nat. Rev. Microbiol.*, 2004, **2**, 95–108.
6 A. Aguilera, S. C. Manrubia, F. Gomez, N. Rodriguez and R. Amils, *Appl. Environ. Microbiol.*, 2006, **72**, 5325–5330.
7 A. Aguilera, V. Souza-Egipsy, F. Gómez and R. Amils, *Microb. Ecol.*, 2007, **53**, 294–305.
8 A. García-Moyano, E. Gónzalez-Toril, A. Aguilera and R. Amils, *Syst. Appl. Microbiol.*, 2007, **30**, 601–614.
9 V. Souza-Egipsy, E. Gonzalez-Toril, E. Zettler, L. Amaral-Zetller, R. Amils and A. Aguilera, *Int. Microbiol.*, 2009, **11**, 251–260.
10 A. Aguilera, V. Souza-Egipsy, P. San Martín-Úriz and R. Amils, *Aquat. Toxicol.*, 2008, **88**, 257–266.
11 A. Aguilera, V. Souza-Egipsy, P. San Martín-Úriz and R. Amils, *Appl. Microbiol. Biotechnol.*, 2008, **78**, 1079–1088.
12 Y. Blanco, L. A. Rivas, E. Gonzalez-Toril, M. Ruiz-Bermejo, M. Moreno-Paz, V. Parro, A. Palacin, A. Aguilera and F. Puente-Sanchez, *Sci. Total Environ.*, 2019, **650**, 384–393.
13 B. Nicolaus, M. Kambourova and E. T. Oner, *Environ. Technol.*, 2010, **31**, 1145–1158.
14 A. Poli, G. Anzelmo and B. Nicolaus, *Mar. Drugs*, 2010, **8**, 1779–1802.
15 N. Billings, A. Birjiniuk, T. S. Samad, P. S. Doyle and K. Ribbeck, *Rep. Prog. Phys.*, 2015, **78**, 036601.
16 B. W. Peterson, Y. He, Y. Ren, A. Zerdoum, M. R. Libera, P. K. Sharma, A.-J. van Winkelhoff, D. Neut, P. Stoodley, H. C. van der Mei and H. J. Busscher, *FEMS Microbiol. Rev.*, 2015, **39**, 234–245.
17 V. D. Gordon, M. Davis-Fields, K. Kovach and C. A. Rodesney, *J. Phys. D: Appl. Phys.*, 2017, 50.
18 G. R. d. S. Araujo, N. B. Viana, F. Gomez, B. Pontes and S. Frases, *Cell Surface*, 2019, **5**, 100028.
19 P. Stoodley, Z. Lewandowski, J. D. Boyle and H. M. Lappin-Scott, *Biotechnol. Bioeng.*, 1999, **65**, 83–92.
20 V. Korstgens, H. C. Flemming, J. Wingender and W. Borchard, *Water Sci. Technol.*, 2001, **43**, 49–57.
21 B. W. Towler, C. J. Rupp, A. B. Cunningham and P. Stoodley, *Biofouling*, 2003, **19**, 279–285.
22 T. Shaw, M. Winston, C. J. Rupp, I. Klapper and P. Stoodley, *Phys. Rev. Lett.*, 2004, **93**, 098102.
23 L. I. Brugnoni, M. C. Tarifa, J. E. Lozano and D. Genovese, *Biofouling*, 2014, **30**, 1269–1279.
24 M. C. Tarifa, D. Genovese, J. E. Lozano and L. I. Brugnoni, *Biofouling*, 2018, **34**, 74–85.
25 E. Eteshola, M. Karpasas, S. Arad and M. Gottlieb, *Acta Polym.*, 1998, **49**, 549–556.
26 I. W. Sutherland, in *Microbial extracellular polymeric substances. Characterizacion, structure and function*, ed. J. Wingender, T. R. Neu and H.-C. Flemming, Springer-Verlang, Berlin-Heidelberg, 1999, pp. 73–92.
27 G.-P. Sheng, H.-Q. Yu and X.-Y. Li, *Biotechnol. Adv.*, 2010, **28**, 882–894.
28 S. D. Weber, W. Ludwig, K. H. Schleifer and J. Fried, *Appl. Environ. Microbiol.*, 2007, **73**, 6233–6240.
29 D. G. Allison, *Biofouling*, 2003, **19**, 139–150.
30 D. M. Paterson, R. M. Crawford and C. Little, *J. Exp. Mar. Biol. Ecol.*, 1986, **95**, 279–289.
31 C. Défarge, J. Trichet, A. Maurin, M. Robert, J. Tribble and F. J. Sansone, *J. Sedim. Petrol.*, 1996, **66**, 935–947.
32 V. Souza-Egipsy, C. Ascaso and L. G. Sancho, *Mycol. Res.*, 2002, **106**, 1367–1374.
33 J. Wierzchos, M. Berlanga, C. Ascaso and R. Guerrero, *Int. Microbiol.*, 2006, **9**, 289–295.
34 N. Kovac, P. Mozetic, J. Trichet and C. Defarge, *Mar. Biol.*, 2005, **147**, 261–271.
35 R. I. Amann, W. Ludwig and K.-H. Schleifer, *Microbiol. Rev.*, 1995, **59**, 143–169.
36 W. L. Jones, M. P. Sutton, L. McKittrick and P. S. Stewart, *Biofouling*, 2011, **27**, 207–215.
37 A. Jaishankar and G. H. McKinley, *Proceedings of the Royal Society A Mathematical Physical and Engineering Sciences*, 2013, 469.
38 G. W. S. Blair, The role of psychophysics in rheology, *J. Colloid Sci.*, 1947, **2**(1), 21–32.
39 T. J. Faber, A. Jaishankar and G. H. McKinley, *Food Hydrocolloids*, 2017, **62**, 311–324.
40 T. J. Faber, A. Jaishankar and G. H. McKinley, *Food Hydrocolloids*, 2017, **62**, 325–339.
41 T. F. Tadros, *Adv. Colloid Interface Sci.*, 1996, **68**, 97–200.
42 J. D. F. Ramsay, S. R. Daish and C. J. Wright, *Faraday Discuss.*, 1978, **65**, 65–75.
43 J. D. F. Ramsay, *J. Colloid Interface Sci.*, 1986, **109**, 441–447.
44 V. Souza-Egipsy, M. Altamirano, R. Amils and A. Aguilera, *Environ. Microbiol.*, 2011, **13**, 2351–2358.
45 P. Stoodley, K. Sauer, D. G. Davies and J. W. Costerton, *Annu. Rev. Microbiol.*, 2002, **56**, 187–209.
46 Y. Chisti, in *Handbook of Microalgae-Based Processes and Products*, ed. E. Jacob-Lopes, M. M. Maroneze, M. I. Queiroz and L. Q. Zepka, Academic Press, London, 2020, pp. 3–23.
47 M. Consalvey, D. M. Paterson and G. J. C. Underwood, *Diatom Res.*, 2004, **19**, 181–202.
48 O. Lieleg, M. Caldara, R. Baumgaertel and K. Ribbeck, *Soft Matter*, 2011, **7**, 3307–3314.
49 K. Hyun, S. H. Kim, K. H. Ahn and S. J. Lee, *J. Non-Newtonian Fluid Mech.*, 2002, **107**, 51–65.
50 A. Alghooneh, S. M. A. Razavi and S. Kasapis, *J. Text. Stud.*, 2019, **50**, 520–538.
51 S. Kunz, M. Pawlik, W. Schaertl and S. Seiffert, *Colloid Polym. Sci.*, 2018, **296**, 1341–1352.
52 L. Martinetti, O. Carey-De la Torre, K. S. Schweizer and R. H. Ewoldt, *Macromolecules*, 2018, **51**, 8772–8789.

